ChemPubSoc Europe

DOI: 10.1002/chem.201900673

CHEMISTRY
A European Journal
Full Paper

Copper Catalysis

The Mechanism of Copper-Catalyzed Trifunctionalization of Terminal Allenes

Hong Ki Kim,[a, b] Manoj V. Mane,[a, b] John Montgomery,*[c] and Mu-Hyun Baik*[a, b]

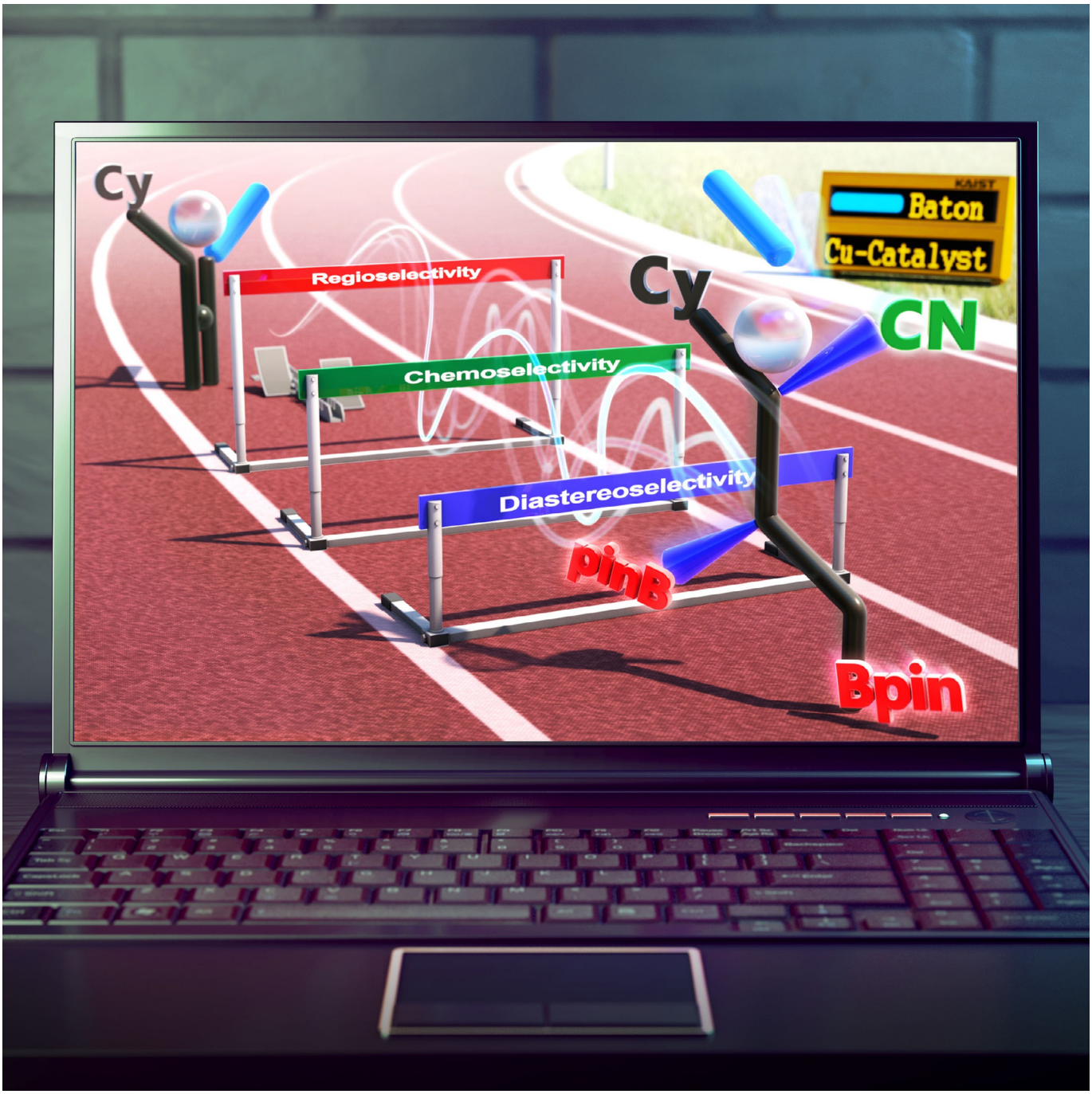

Abstract: A highly selective copper-catalyzed trifunctionalization of allenes has been established based on diborylation/cyanation with bis(pinacolato)diboron (B_2pin_2) and *N*-cyano-*N*-phenyl-*p*-toluenesulfonamide (NCTS). The Cu-catalyzed trifunctionalization of terminal allenes is composed of three catalytic reactions (first borocupration, electrophilic cyanation, and second borocupration) that provide a densely functionalized product with regio-, chemo- and diastereoselectivity. Allene substrates have multiple reaction-sites, and the selectivities are determined by the suitable interactions (e.g., electronic and steric demands) between the catalyst and substrates. We employed DFT calculations to understand the cascade copper-catalyzed trifunctionalization of terminal allenes, providing densely-functionalized organic molecules with outstanding regio-, chemo- and diastereoselectivity in high yields. The selectivity challenges presented by cumulated π-systems are addressed by systematic computational studies; these give insight to the catalytic multiple-functionalization strategies and explain the high selectivities that we see for these reactions.

Introduction

Transition-metal-catalyzed functionalization of boron-containing σ-bonds to carbon–carbon multiple bonds is an effective strategy for the formation of densely functionalized organic molecules.[1] In particular, transition-metal boryl complexes play a key role in a range of borylation reactions, such as, C–H borylation, hydroboration, diboration, and other B–X addition reactions on unsaturated organic substrates.[1f,2] More specifically, allene substrates have been investigated previously, motivated by the variety of structural motifs and functional value that allenes present for access to natural products, pharmaceuticals, and organic materials.[2e,f,3] Trifunctionalization processes have the potential to provide practical and powerful solutions for accessing valuable organic molecules with intriguing selectivities and high yields,[1b-e,4] but the strategy remains underdeveloped compared to other reaction types that show similar versatility. Recently, Ma and Ito reported the borocupration reaction of allenes with B_2pin_2 based on both experimental and theoretical studies.[5] Although the borometalation processes of substrates that possess two or more π-bonds have considerable potential in this regard, their application in trifunctionalization processes needs to be further explored.

We have previously reported that functionalized products with high degrees of regio-, chemo- and diastereoselectivity are efficiently synthesized through a copper-catalyzed cascade trifunctionalization of terminal allenes derived from diborylation and cyanation, as depicted in Scheme 1.[6] Based on the experimental study, a putative mechanism was proposed to involve a series of diborylation and cyanation on the π-systems of the allene substrates. Most importantly, we were able to isolate an alkenyl intermediate, which is proposed to give the trifunctionalized final product. Whereas the overall sequence of the reaction appears to be clear, many important details remain poorly understood. For example, it is not at all clear which features govern the various selectivities that have been observed and that make these reactions synthetically attractive.

In this study, we employ DFT calculations to understand the mechanism for the copper-catalyzed trifunctionalization of cyclohexyl allene in detail. The aim of this study is to explain the observed triple-selectivities as shown in Scheme 1 and to construct a complete mechanistic framework that will expedite the rational design of the next generation of new catalytic reactions.

Computational Methods

All calculations were performed by DFT calculations[7] as implemented in the Jaguar 9.1 suite[8] of ab initio quantum chemistry programs. Geometry optimizations to the stationary points as well as the transition state (TS) optimization to the saddle points were performed with the B3LYP[9] hybrid exchange and correlation functional including Grimme's D3 dispersion correction.[10] The 6-31G** basis set[11] was used for all atoms except for copper, which was represented by the Los Alamos LACVP** basis set,[12] including effective core potentials. The energies of the optimized structures were reevaluated by single-point calculations on each optimized geometry using Dunning's correlation consistent triple-ζ basis set cc-pVTZ(-f)[13] that includes a double set of polarization functions. Copper atom was represented by using a triple-ζ version of LACVP**, where the exponent of the basis functions were decontracted to mimic the flexibility of the triple-ζ basis. Analytical vibrational frequencies within the harmonic oscillator approximation were computed with the B3LYP-D3/6-31G** level to confirm proper convergence to well-defined minima and saddle points on the potential energy surface. Solvation energies were evaluated by a

[a] *H. K. Kim, Dr. M. V. Mane, Prof. Dr. M.-H. Baik*
Department of Chemistry
Korea Advanced Institute of Science and Technology (KAIST)
Daejeon 34141 (Republic of Korea)
E-mail: mbaik2805@kaist.ac.kr

[b] *H. K. Kim, Dr. M. V. Mane, Prof. Dr. M.-H. Baik*
Center for Catalytic Hydrocarbon Functionalizations,
Institute for Basic Science (IBS), Daejeon 34141 (Republic of Korea)

[c] *Prof. Dr. J. Montgomery*
Department of Chemistry, University of Michigan
930 North University Avenue, Ann Arbor, Michigan 48109-1055 (USA)
E-mail: jmontg@umich.edu

Supporting information, including computed energy components, Cartesian coordinates, vibrational frequencies of all of the DFT-optimized structures, and the ORCID identification number(s) for the author(s) of this article can be found under:
https://doi.org/10.1002/chem.201900673.

Part of a Special Issue in honor of the 20th IUPAC International Symposium on Organometallic Chemistry directed towards Organic Synthesis (OMCOS 20). To view the complete issue, visit Issue 40.

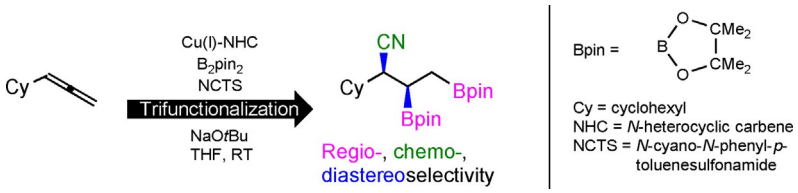

Scheme 1. The cascade copper-catalyzed trifunctionalization process—a triple-selective functionalization of cyclohexyl allene.

self-consistent reaction field (SCRF) approach based on accurate numerical solutions of the Poisson–Boltzmann equation.[14] These solvation calculations were carried out with the B3LYP-D3/6-31G** level at the optimized gas-phase geometry employing the dielectric constant of $\varepsilon = 7.6$ for tetrahydrofuran (THF). As is the case for all continuum models, the solvation energies are subject to empirical parametrization of the atomic radii that are used to generate the solute surface. We employed the standard set of optimized radii in Jaguar for H (1.150 Å), B (2.042 Å), C (1.900 Å), N (1.600 Å), O (1.600 Å), Na (1.491 Å), S (2.070 Å), Cl (1.974 Å), and Cu (1.748 Å).[15] The free energy in solution-phase *G*(sol) was calculated as follows:

$$G(\text{sol}) = G(\text{gas}) + \Delta G(\text{solv}) \quad (1)$$

$$G(\text{gas}) = H(\text{gas}) - TS(\text{gas}) \quad (2)$$

$$H(\text{gas}) = E(\text{SCF}) + \text{ZPE} \quad (3)$$

$$\Delta E(\text{SCF}) = \Sigma E(\text{SCF})\ \text{for products} - \Sigma E(\text{SCF})\ \text{for reactants} \quad (4)$$

$$\Delta G(\text{sol}) = \Sigma G(\text{sol})\ \text{for products} - \Sigma G(\text{sol})\ \text{for reactants} \quad (5)$$

G(gas) is the free energy in the gas phase; *G*(solv) is the free energy of solvation as computed by the continuum solvation model; *H*(gas) is the enthalpy in gas phase; *T* is the temperature (298.15 K); *S*(gas) is the entropy in the gas phase; *E*(SCF) is the self-consistent field energy, that is, raw electronic energy as computed from the SCF procedure; and ZPE is the zero-point energy. Note that by entropy here we refer specifically to the vibrational/rotational/translational entropy of the solute(s). The entropy of the solvent is incorporated implicitly in the continuum solvation model. Transition state structures were obtained from the quadratic synchronous transit (QST) search methods.[16]

Results and Discussion

Mechanism

The proposed reaction pathway for the Cu^{I}-catalyzed trifunctionalization of the allene substrate is outlined in Scheme 2 and consists of three major steps that govern the regio-, chemo- and diastereoselectivities. For the purpose of constructing a model reaction energy profile, which is shown in Figure 2, we chose to employ the cyclohexyl allene substrate, which was experimentally shown to selectively form the 1,2,3-trifunctionalized product **18** in high yields. In general, borocupration reactions are thought to involve N-heterocyclic carbene (NHC) copper-boryl complex **7** as the active species with a range of reported NHC ligands, such as 1,3-bis(2,4,6-trimethylphenyl)imidazol-2-ylidene (IMes), 1,3-bis(2,4,6-trimethylphenyl)- 4,5-dihydroimidazol-2-ylidene (SiMes), 1,3-bis(2,6-diisopropylphenyl)imidazol-2-ylidene (IPr), and 1,3-dicyclohexylimidazol-2-ylidene (ICy).[17] Among them, ICy was found to offer the best combination of high yields and triple selectivities for the product **18**. The catalytic cycles proceed as summarized in Scheme 2, with the precatalyst ICyCu–Cl, B_2pin_2, and NaO*t*Bu reacting to generate ICyCu–Bpin species **7** in THF.

The formation of the catalytically active species **7** deserves some attention, as it is the key intermediate that starts the catalytic cycle and is responsible for two different borylation cycles during the reaction cascade. It is generated from the precatalyst LCu–Cl with NaO*t*Bu and B_2pin_2, as illustrated in Figure 1.[18] Starting from reactants **1** and **2**, ligand exchange gives a thermodynamically stable LCu–O*t*Bu complex **5** and sodium chloride, which can undergo a σ-bond metathesis reaction where the Cu–O and B–B bonds are cleaved and Cu–B and O–B bonds are formed through a typical four-membered ring transition state **3-TS** at a relative energy of 16.2 kcal mol^{-1} to afford the stable intermediate complex **7** at −15.6 kcal mol^{-1}. We expect this reaction to be irreversible and rapid, given the low barrier and large exothermic driving force.

As illustrated in Figure 2, the catalytic cycle starts with species **7** adding across a terminal double bond of the allene to form an intermediate **9a**, a Cu-η^2-allene π-complex, at a rela-

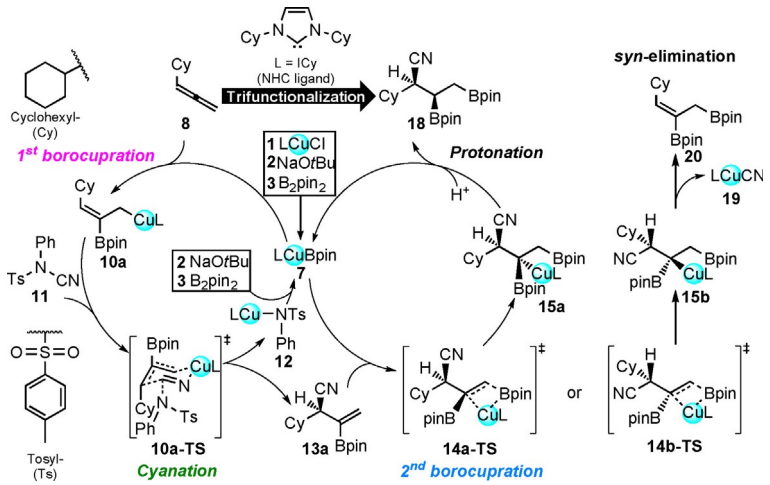

Scheme 2. Overview of the mechanism for the Cu-catalyzed trifunctionalization of cyclohexyl allene.

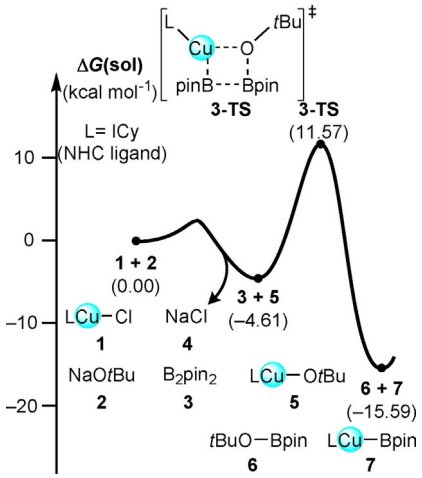

Figure 1. Energy profiles for precatalyst activation.

tive energy of 4.6 kcal mol^{-1}, making this step endergonic by 11.0 kcal mol^{-1}. The insertion of the allene into the Cu–B bond is surprisingly easy from this π-adduct; it only requires an additional 7.7 kcal mol^{-1} to afford an overall barrier of 18.7 kcal mol^{-1} for the insertion from intermediate **7**. The inserted species is the olefin intermediate **10a**, which we were able to locate at −45.4 kcal mol^{-1}, rendering this insertion step irreversible. Note that the regiochemical outcome, that is, which double bonds of the allene that are functionalized, is determined at this step, as will be discussed in greater detail below. Our calculations suggest that intermediate **10a** is not observed experimentally, because the cyanation in the next step is associated with a very low barrier of only 13.9 kcal mol^{-1} traversing the transition state **10a-TS**. *Ortho*-cyanation of a benzyl copper species by reagent **11** was first described by Buchwald[19] and was computationally studied by Liu.[20] Given that the cyanating reagent is offered in sufficient quantities, this step is expected to be fast, preventing the accumulation of **10a** in the reaction mixture. The product of the cyanation is intermediate **13a**, located at a free energy of −83.5 kcal mol^{-1}, rendering the cyanation step also irreversible with an energetic driving force of **10a**→**13a** to be 38.1 kcal mol^{-1}. For the final step of the cascade reaction, intermediate **13a** must be re-engaged by the catalytically active species **7** to facilitate the second borocupration reaction. Our calculations suggest that this step is also facile with an activation barrier of only 11.4 kcal mol^{-1} associated with the transition state **14a-TS** to give the product complex **15a**, but since the concentration of **7** is low, the rate of this step is expected to be slow compared to the other steps with similar or even slightly higher barriers. As a consequence, the alkenyl intermediate **13a** may be accumulated during the catalytic reaction and can be isolated, as previously found. Furthermore, we have observed experimentally that independently prepared **13a** is converted to the expected product **18**, and have suggested that **13a** is not the final product because the second borocupration is a highly exothermic reaction with an energetic driving force of 15.7 kcal mol^{-1} and the lowest activation barrier is about 11 kcal mol^{-1} in the copper-catalyzed trifunctionalization reaction based on DFT calculations. Finally, protonation of **15a** gives the trifunctionalized cyanation/diborylation product **18**. Figure 2 also indicates which step is responsible for the regio-, chemo- and

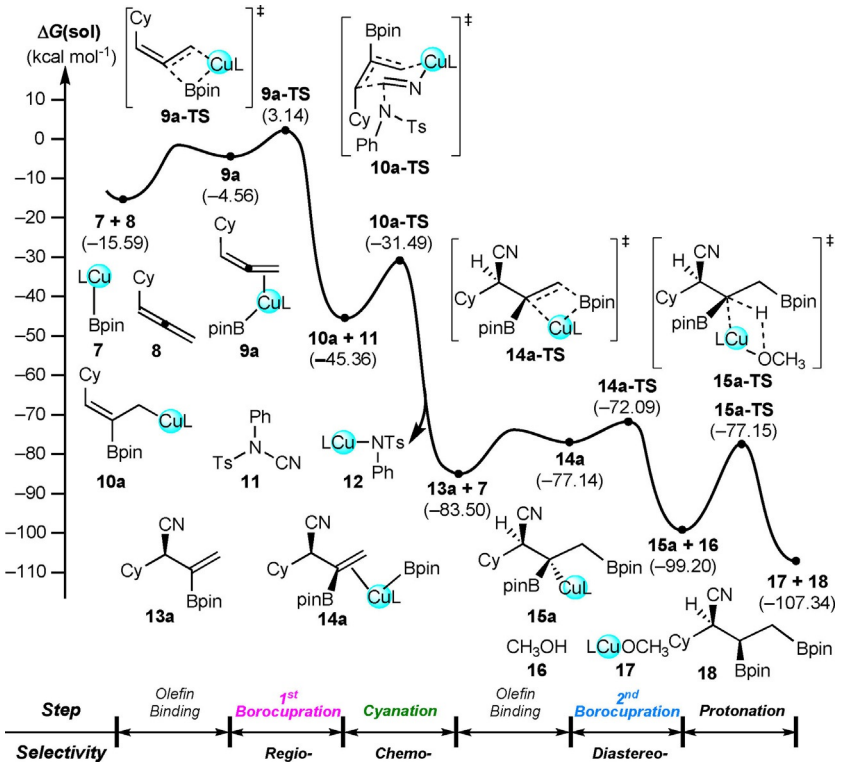

Figure 2. Overall energy profiles for Cu-catalyzed trifunctionalization of terminal allenes.

diastereoselectivity, namely, the first borylation, the cyanation, and the second borylation, respectively. These features are discussed in detail below.

Regioselective first borocupration

As discussed above, the first borocupration of the allene substrate determines the regioselectivity in the cascade reaction. In principle, there are four possible ways of inserting the cyclohexyl allene substrate **8** into the Cu–B bond, as summarized in Figure 3. Within an energy range of about 3 kcal mol^{-1}, we were able to locate four structural isomers of the reactant π-complex, where **9a** and **9b** have the copper catalyst bound at the distal double bond from the cyclohexyl group, adopting two different orientations of the NHC ligand. Intermediates **9c** and **9d** are the analogous π-complexes, in which Cu coordinates to the proximal double bond. These four structural isomers offer entries into the four different regiochemical reaction channels that will produce regioisomeric borocupration products **10(a–d)**, as illustrated in Figure 3. The activation barriers associated with these four channels and the transition states **9(a–d)-TS** are remarkably different at 18.7, 21.0, 23.3, and 50.3 kcal mol^{-1}, respectively. The trajectory with the lowest barrier associated with **9a-TS** gives intermediate **10a**, which is also the lowest in energy by about 8–11 kcal mol^{-1} among all regioisomers at −45.4 kcal mol^{-1}.

To understand the origin of the regioselectivity during the first borocupration, we examined each of the transition states **9(a–d)-TS** on the four different regiochemical reaction channels. This analysis illustrated that there are two features that determine the energies of these transition states. First, the insertion of the boryl moiety to form the C–B bond favors the stronger Lewis basic sp carbon of the allene over the weaker Lewis basic sp^2 carbon as highlighted in Figure 3. This finding is easy to understand since the boryl group acts as a Lewis acid in this bond formation. Thus, the transition states **9a-TS** and **9c-TS** are electronically favored over transition states **9b-TS** and **9d-TS**. The second determining factor is the steric demand enforced by the cyclohexyl functionalities flanking the N-heterocyclic carbene ligand and the terminal cyclohexyl group of the allene substrate. As depicted in Figure 4, these

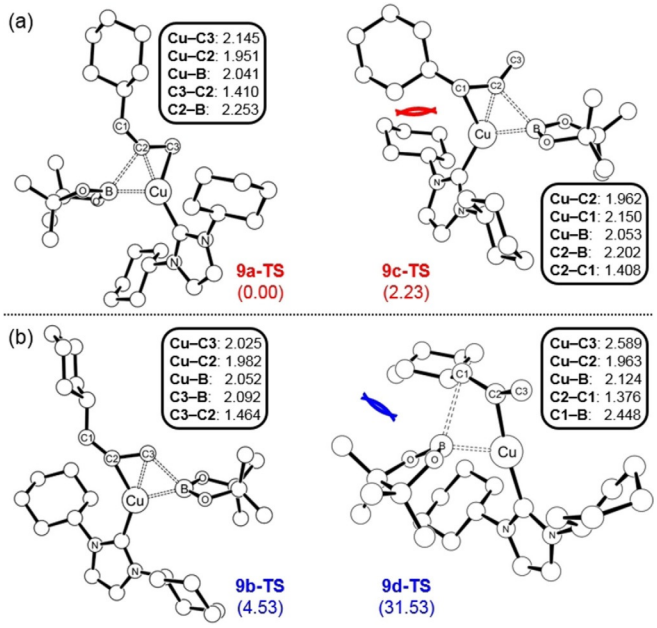

Figure 4. For the first borocupration, four possible transition state structures forming the C–B bond related to sp carbon (a) and sp^2 carbon (b). Hydrogen atoms bound to carbon atoms are omitted for the sake of clarity. All bond lengths are in Å. Relative free energy differences (kcal mol^{-1}) are in parenthesis.

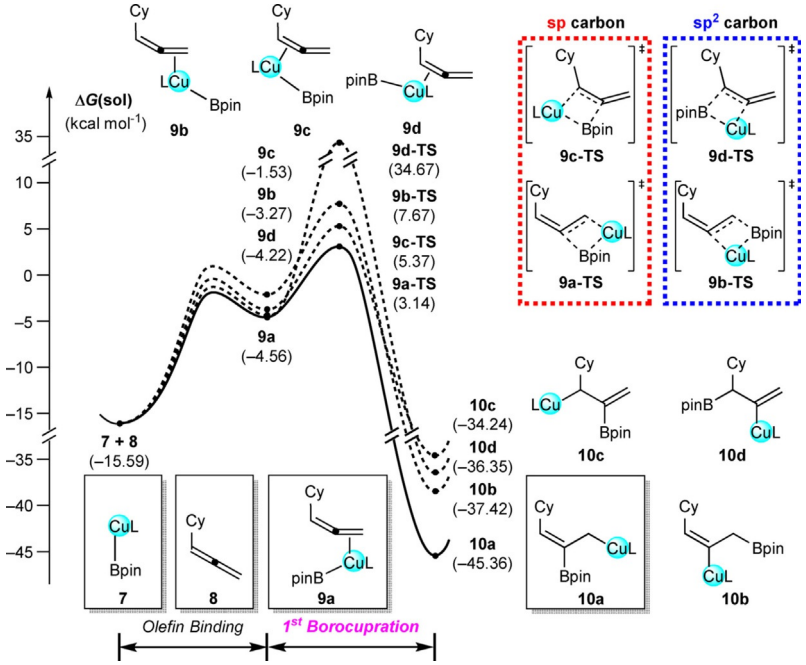

Figure 3. Energy profiles for four possible regioisomeric pathways of the first borocupration related to the regioselectivity.

sterically demanding groups are oriented away from each other in **9a-TS** and **9b-TS**. In the other two transition states, the cyclohexyl groups cause a steric clash, giving rise to higher energies. Consequently, **9a-TS** is the lowest in energy. For similar reasons, intermediate **10a** is about 8 kcal mol^{-1} lower in energy than **10b**. Therefore, the formation of the σ-allyl complex **10a** is kinetically and thermodynamically the most affordable.

Stereoselective cyanation

After undergoing borocupration, the NCTS substrate can act as an electrophilic cyanating agent to afford cyanation products in high yields with excellent selectivity.[19–21] As shown in Figure 5, the barrier associated with the formation of **10a-TS** is only 14.0 kcal mol^{-1} and is expected to be fast in realistic reaction conditions. The transition state adopts a six-membered ring conformation as the copper center coordinates to the terminal nitrogen atom of the cyano group. Consequently, by placing the cyclohexyl group in the axial position, a relaxed geometry without steric stress is allowed through the six-membered ring. Furthermore, we found two possible conformational isomers, **13a** and **13b**, that may be formed from intermediate **11** via transition state **10a-TS**. The rotamers **13a** and **13b** can explain the experimentally observed stereoselectivity in the second borocupration step.

Regio- and diastereoselective second borocupration

Addition of the boryl–copper compound **7** to the olefin occurs in a regio- and stereoselective manner. The stereocontrol is imposed by the sterically demanding interaction between the cyclohexyl group of the alkene substrate and species **7**. As illustrated in Figure 6a, the boryl–copper complex **7** reacts with **13a** on the *si* face because the cyclohexyl group effectively blocks the *re* face. Conversely, in **13b** the *re* face is blocked by the cyclohexyl moiety, forcing the borocupration to proceed at the *si* face. Four borocuparated products **15a**, **15b**, **15a′**, and **15b′** are possible, as shown in Figures 6 and Figure S1. The intermediate **13a** first forms the π-complex with **7**, which is about 6 kcal mol^{-1} uphill to afford the two conformers **14a** and **14a′**. The borocupration is exceedingly facile and reaching **14a-TS** only requires an additional 5.0 kcal mol^{-1} to give a total barrier of 11.4 kcal mol^{-1} for the formation of **15a**. The reaction leading to the alternative regioisomer **15a′** requires more energy with a barrier of 19.6 kcal mol^{-1}. This regiochemical outcome is easy to understand, as the double bond is likely cleaved in a heterolytic fashion through which the terminal carbon becomes negatively polarized and well matched with the boryl functionality that acts as a Lewis acid. The regiocontrol is also operative for intermediates **14b** and **14b′**, thus, favoring the formation of **15b** with a barrier of 13.2 kcal mol^{-1}. Comparing the diastereoisomers **15a** and **15b**, our calculations predict a nearly 2 kcal mol^{-1} kinetic preference for the formation of **15a**, which is again in excellent agreement with experimental observations. As discussed above, protonation of **15a** affords the final trifunctionalized product **18**.

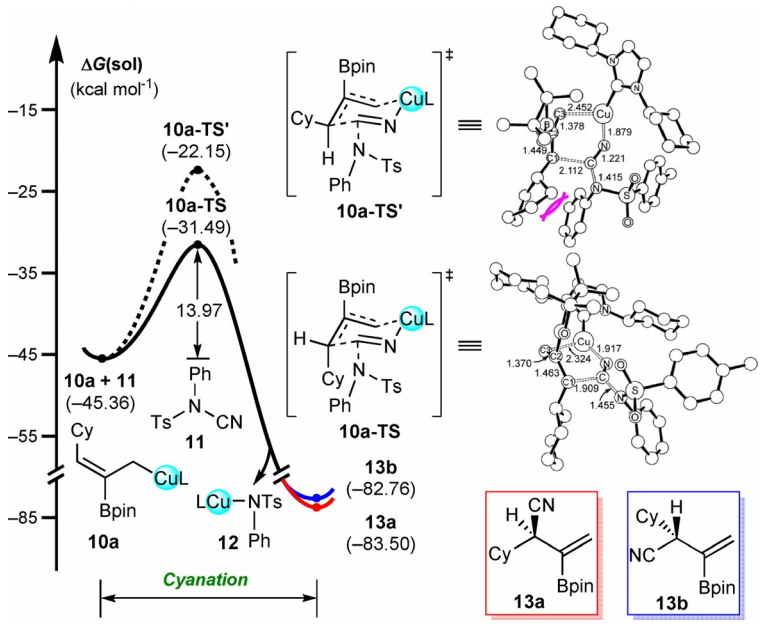

Figure 5. Energy profiles of the cyanation pathway. Hydrogen atoms bound to carbon atoms are omitted for the sake of clarity. All bond lengths are in Å.

Conclusion

In summary, our calculations have revealed a detailed mechanism for the Cu-catalyzed trifunctionalization of cyclohexyl allene employing B_2pin_2 and NCTS as borylation and cyanation sources, respectively. We present, for the first time, a detailed mechanism for this fascinating, efficient cascade reaction that generates the cyanation/diborylation product with exceptional regio-, chemo- and diastereoselectivity. Although the sequence of the three reactions occurs in a highly orchestrated fashion, the regio- and stereoselectivities determined in each of the reaction steps are easily rationalized by this study. Specifically, the regiocontrol of the two borocupration steps is determined by significantly different effects. The first borocupration is controlled mainly though sterical demands and the second through electronic effects. The diastereoselectivity follows a classical strategy of sterical blocking one of the reactive faces of the olefin by placing the cyclohexyl functionality on that molecular face. This investigation offers a precise mechanistic blueprint and serves as a platform for future explorations and rational catalyst design. Applications of these concepts will be pursued in our laboratories and reported in due course.

Acknowledgements

We thank the Institute for Basic Science (IBS-R10-A1) in Korea and the US National Science Foundation (CHE-1565837) for financial support.

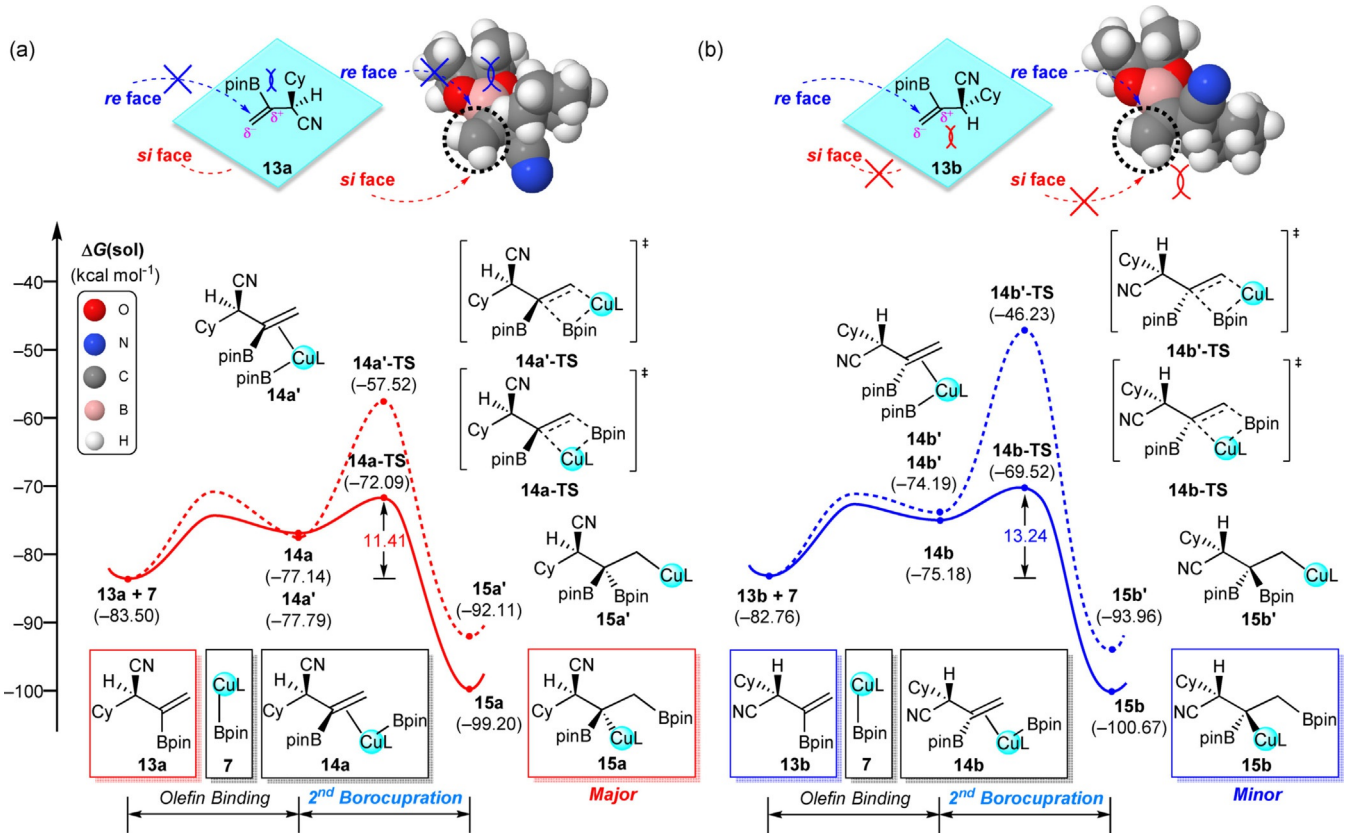

Figure 6. Energy profiles for the second borocupration pathway, related to the regio- and diastereoselectivity derived from two conformational isomers, **13a** and **13b**.

Conflict of interest

The authors declare no conflict of interest.

Keywords: borylation · copper catalysis · cyanation · density functional theory · selectivities · trifunctionalization

[1] a) N. F. Pelz, J. P. Morken, *Org. Lett.* **2006**, *8*, 4557–4559; b) G. R. Clark, P. M. Johns, W. R. Roper, T. Söhnel, L. J. Wright, *Organometallics* **2011**, *30*, 129–138; c) Q. Feng, K. Yang, Q. Song, *Chem. Commun.* **2015**, *51*, 15394–15397; d) Y. Li, D. Qiu, R. Gu, J. Wang, J. Shi, Y. Li, *J. Am. Chem. Soc.* **2016**, *138*, 10814–10817; e) S. Ni, W. Sha, L. Zhang, C. Xie, H. Mei, J. Han, Y. Pan, *Org. Lett.* **2016**, *18*, 712–715; f) K. Semba, M. Shinomiya, T. Fujihara, J. Terao, Y. Tsuji, *Chem. Eur. J.* **2013**, *19*, 7125–7132.

[2] a) S. Ma, *Acc. Chem. Res.* **2009**, *42*, 1679–1688; b) R. Zimmer, C. U. Dinesh, E. Nandanan, F. A. Khan, *Chem. Rev.* **2000**, *100*, 3067–3126; c) S. Ma, *Acc. Chem. Res.* **2003**, *36*, 701–712; d) S. Ma, *Chem. Rev.* **2005**, *105*, 2829–2872; e) N. Krause, C. Winter, *Chem. Rev.* **2011**, *111*, 1994–2009; f) S. Yu, S. Ma, *Angew. Chem. Int. Ed.* **2012**, *51*, 3074–3112; *Angew. Chem.* **2012**, *124*, 3128–3167; g) R. K. Neff, D. E. Frantz, *Tetrahedron* **2015**, *71*, 7–18.

[3] a) A. S. K. Hashmi, *Angew. Chem. Int. Ed.* **2000**, *39*, 3590–3593; *Angew. Chem.* **2000**, *112*, 3737–3740; b) J. A. Marshall, K. G. Pinney, *J. Org. Chem.* **1993**, *58*, 7180–7184; c) J. A. Marshall, G. S. Bartley, E. M. Wallace, *J. Org. Chem.* **1996**, *61*, 5729–5735; d) K. Yeung, F. J. T. Talbot, G. P. Howell, A. P. Pulis, D. J. Procter, *ACS Catal.* **2019**, *9*, 1655–1661.

[4] a) X.-Y. Duan, X.-L. Yang, R. Fang, X.-X. Peng, W. Yu, B. Han, *J. Org. Chem.* **2013**, *78*, 10692–10704; b) J. Liu, M. Skaria, P. Sharma, Y.-W. Chiang, R.-S. Liu, *Chem. Sci.* **2017**, *8*, 5482–5487; c) R. Banerjee, N. J. Pace, D. R. Brown, E. Weerapana, *J. Am. Chem. Soc.* **2013**, *135*, 2497–2500; d) K.-L. Zheng, W.-M. Shu, J.-R. Ma, Y.-D. Wu, A.-X. Wu, *Org. Lett.* **2016**, *18*, 3526–3529; e) A. G. Kutateladze, J. L. Kice, T. G. Kutateladze, N. S. Zefirov, *J. Org. Chem.* **1993**, *58*, 995–996.

[5] a) W. Yuan, X. Zhang, Y. Yu, S. Ma, *Chem. Eur. J.* **2013**, *19*, 7193–7202; b) Y. Ozawa, H. Iwamoto, H. Ito, *Chem. Commun.* **2018**, *54*, 4991–4994.

[6] W. Zhao, J. Montgomery, *J. Am. Chem. Soc.* **2016**, *138*, 9763–9766.

[7] R. G. Parr, Y. Weitao, *Density-Functional Theory of Atoms and Molecules*, Oxford University Press, **1994**.

[8] A. D. Bochevarov, E. Harder, T. F. Hughes, J. R. Greenwood, D. A. Braden, D. M. Philipp, D. Rinaldo, M. D. Halls, J. Zhang, R. A. Friesner, *Int. J. Quantum Chem.* **2013**, *113*, 2110–2142.

[9] a) J. C. Slater, *Quantum Theory of Molecules and Solids*, McGraw-Hill: New York, **1974**; b) S. H. Vosko, L. Wilk, M. Nusair, *Can. J. Phys.* **1980**, *58*, 1200–1211; c) A. D. Becke, *Phys. Rev. A* **1988**, *38*, 3098–3100; d) C. Lee, W. Yang, R. G. Parr, *Phys. Rev. B* **1988**, *37*, 785–789.

[10] S. Grimme, J. Antony, S. Ehrlich, H. Krieg, *J. Chem. Phys.* **2010**, *132*, 154104.

[11] R. Ditchfield, W. J. Hehre, J. A. Pople, *J. Chem. Phys.* **1971**, *54*, 724–728.

[12] a) P. J. Hay, W. R. Wadt, *J. Chem. Phys.* **1985**, *82*, 270–283; b) W. R. Wadt, P. J. Hay, *J. Chem. Phys.* **1985**, *82*, 284–298; c) P. J. Hay, W. R. Wadt, *J. Chem. Phys.* **1985**, *82*, 299–310.

[13] T. H. Dunning Jr., *J. Chem. Phys.* **1989**, *90*, 1007–1023.

[14] a) B. Marten, K. Kim, C. Cortis, R. A. Friesner, R. B. Murphy, M. N. Ringnalda, D. Sitkoff, B. Honig, *J. Phys. Chem.* **1996**, *100*, 11775–11788; b) S. R. Edinger, C. Cortis, P. S. Shenkin, R. A. Friesner, *J. Phys. Chem. B* **1997**, *101*, 1190–1197; c) M. Friedrichs, R. Zhou, S. R. Edinger, R. A. Friesner, *J. Phys. Chem. B* **1999**, *103*, 3057–3061.

[15] A. A. Rashin, B. Honig, *J. Phys. Chem.* **1985**, *89*, 5588–5593.

[16] C. Peng, H. B. Schlegel, *Isr. J. Chem.* **1993**, *33*, 449–454.

[17] a) K. Yeung, R. E. Ruscoe, J. Rae, A. P. Pulis, D. J. Procter, *Angew. Chem. Int. Ed.* **2016**, *55*, 11912–11916; *Angew. Chem.* **2016**, *128*, 12091–12095; b) Y. Huang, K. B. Smith, M. K. Brown, *Angew. Chem. Int. Ed.* **2017**, *56*, 13314–13318; *Angew. Chem.* **2017**, *129*, 13499–13503; c) F. Cheng, W. Lu, W. Huang, L. Wen, M. Li, F. Meng, *Chem. Sci.* **2018**, *9*, 4992–4998;

d) H. Jang, F. Romiti, S. Torker, A. H. Hoveyda, *Nat. Chem.* **2017**, *9*, 1269 – 1275; e) R. Sakae, K. Hirano, M. Miura, *J. Am. Chem. Soc.* **2015**, *137*, 6460 – 6463; f) R. Corberán, N. W. Mszar, A. H. Hoveyda, *Angew. Chem. Int. Ed.* **2011**, *50*, 7079 – 7082; *Angew. Chem.* **2011**, *123*, 7217 – 7220.

[18] a) D. S. Laitar, P. Müller, J. P. Sadighi, *J. Am. Chem. Soc.* **2005**, *127*, 17196 – 17197; b) Y. Lee, A. H. Hoveyda, *J. Am. Chem. Soc.* **2009**, *131*, 3160 – 3161.

[19] Y. Yang, S. L. Buchwald, *Angew. Chem. Int. Ed.* **2014**, *53*, 8677 – 8681; *Angew. Chem.* **2014**, *126*, 8821 – 8825.

[20] Y. Yang, P. Liu, *ACS Catal.* **2015**, *5*, 2944 – 2951.

[21] a) W. Zhao, J. Montgomery, *Angew. Chem. Int. Ed.* **2015**, *54*, 12683 – 12686; *Angew. Chem.* **2015**, *127*, 12874 – 12877; b) T. Jia, Q. He, R. E. Ruscoe, A. P. Pulis, D. J. Procter, *Angew. Chem. Int. Ed.* **2018**, *57*, 11305 – 11309; *Angew. Chem.* **2018**, *130*, 11475 – 11479.

Manuscript received: February 12, 2019
Revised manuscript received: March 20, 2019
Version of record online: April 30, 2019